Front. Earth Sci. 2019, 13(2): 327–335
https://doi.org/10.1007/s11707-018-0734-8

RESEARCH ARTICLE

Land use and land cover classification using Chinese GF-2 multispectral data in a region of the North China Plain

Kun JIA[1,2], Jingcan LIU[1,2], Yixuan TU[1,2], Qiangzi LI (✉)[3], Zhiwei SUN[4], Xiangqin WEI[3], Yunjun YAO[1,2], Xiaotong ZHANG[1,2]

1 State Key Laboratory of Remote Sensing Science, Jointly Sponsored by Beijing Normal University and Institute of Remote Sensing and Digital Earth of Chinese Academy of Sciences, Beijing 100875, China
2 Beijing Engineering Research Center for Global Land Remote Sensing Products, Faculty of Geographical Science, Beijing Normal University, Beijing 100875, China
3 Institute of Remote Sensing and Digital Earth, Chinese Academy of Sciences, Beijing 100101, China
4 Beijing Geoway Times Software Technology Co., Ltd., Beijing 100043, China

Abstract The newly launched GF-2 satellite is now the most advanced civil satellite in China to collect high spatial resolution remote sensing data. This study investigated the capability and strategy of GF-2 multispectral data for land use and land cover (LULC) classification in a region of the North China Plain. The pixel-based and object-based classifications using maximum likelihood (MLC) and support vector machine (SVM) classifiers were evaluated to determine the classification strategy that was suitable for GF-2 multispectral data. The validation results indicated that GF-2 multispectral data achieved satisfactory LULC classification performance, and object-based classification using the SVM classifier achieved the best classification accuracy with an overall classification accuracy of 94.33% and kappa coefficient of 0.911. Therefore, considering the LULC classification performance and data characteristics, GF-2 satellite data could serve as a valuable and reliable high-resolution data source for land surface monitoring. Future works should focus on improving LULC classification accuracy by exploring more classification features and exploring the potential applications of GF-2 data in related applications.

Keywords land use and land cover, classification, GF-2, North China Plain, multispectral data

1 Introduction

Land use and land cover (LULC) patterns reflect the underlying natural and social processes, which provide important information for modeling and understanding Earth processes and human activities (Liu et al., 2003; Liang, 2008; Yu et al., 2018). Therefore timely, reliable, and objective LULC data at regional and global scales are needed for geoscience, global change, and related studies (Miller et al., 2007; Running, 2008; Gong et al., 2013; Yang et al., 2013). Remote sensing techniques have long been the important means for large area LULC information collection because of their ability to quickly and efficiently collect information about spatial variability occurring on Earth's surface (Hansen et al., 2000; Chen et al., 2015; Gong et al., 2016; Schmidt et al., 2016; Zhang et al., 2017).

Remote sensing data classification is the primary means for LULC monitoring using remote sensing data (Mathur and Foody, 2008; Zhang et al., 2008; Jia et al., 2011). Currently, medium to low spatial resolution remote sensing data are used to classify LULC types at large regional scales because they easily acquire multitemporal data that benefits LULC classification, such as Landsat data and Moderate Resolution Imaging Spectroradiometer (MODIS) data (Friedl and Brodley, 1997; Jia et al., 2014a; Yan and Roy, 2016; Zhong et al., 2016). However, due to the complex natural environment, high spatial resolution remote sensing data are needed for precise LULC classification in China. High spatial resolution LULC maps also serve as a basic information source for natural resource management, such as afforestation assessment and precision agriculture (Gebbers and Adamchuk, 2010; Li et al., 2014). Therefore, generating detailed LULC distribution maps with high spatial resolution is of great significance for land surface monitoring.

Currently, many types of high spatial resolution remote sensing data can be used for LULC classification, such as

Received May 9, 2018; accepted August 26, 2018

E-mail: liqz@radi.ac.cn

RapidEye, Worldview-2 and GeoEye (Adam et al., 2014; Aguilar et al., 2014). In addition to these commercial satellite data, the Chinese GF-2 satellite from the Major National Science and Technology Project of China is now the most advanced civil satellite in China to collect high spatial resolution remote sensing data, which also have great potential for land surface monitoring applications. The GF-2 satellite, known as a member of the China high resolution earth observation system, was launched from the Taiyuan Satellite Launch Centre (Shanxi Province, China) on 19th August 2016, and a large amount of high spatial resolution data have been obtained since then. The GF-2 satellite is in a sun-synchronous orbit at an altitude of 631.5 km and carries two panchromatic/multispectral (P/MS) cameras. The GF-2 multispectral cameras observe solar radiation reflected by the Earth in four spectral channels distributed in the visible and NIR spectral domain ranging from 450 to 890 nm. GF-2 multispectral data have a spatial resolution of 4 m and swath width of 45 km with the two cameras combined, as well as a high frequency revisit time of five days with its side swing capability. The main technical specifications for GF-2 multispectral cameras are shown in Table 1.

The high spatial and temporal resolutions of the GF-2 satellite multispectral data can well satisfy the demand for detailed land surface monitoring and related applications. Furthermore, compared with commercial high spatial resolution satellite data, GF-2 satellite data are freely provided for Chinese land and resource, forestry, and other relevant sectors, which offers great potential for related applications of high spatial resolution remote sensing data. Therefore, assessment of LULC classification performance using GF-2 multispectral data and selection of suitable LULC classification strategy for GF-2 multispectral data is a significant work.

There are three main strategies for remote sensing data classification including pixel-based classification, object-based classification, and subpixel classification, which are appropriate for medium resolution, very high spatial resolution, and low-resolution remote sensing data, respectively (Lu and Weng, 2007; Zhang et al., 2014). The 4 m spatial resolution of GF-2 multispectral data is between the very high spatial resolution and the medium resolution, thus whether a pixel-based or object-based classification strategy is more suitable for LULC classification using this data is also an interesting issue. Therefore, the objectives of this study are to investigate the capability of GF-2 multispectral data for LULC classification in a region of the North China Plain and to determine the appropriate classification strategy for LULC classification using this data. The remainder of the paper is organized as follows. Section 2 presents the study area and the field survey to determine the actual LULC distribution within the study area. Section 3 presents the dataset and data processing. Section 4 provides a detailed description about the methods used in this study. Section 5 shows the classification results and compares the classification performances of different classification strategies. Finally, Section 6 outlines the conclusions.

2 Study area and field survey

The study area is located in the Shandong Province of China (centered at 37°9′N, 117°27′E), which has the typical LULC distribution characteristics in the North China Plain (Fig. 1). The region belongs to the temperate monsoon climatic zone, with an annual precipitation of approximately 587 mm and an annual average temperature of 12.8°C. The climate in this study area has four distinct seasons with rain and warm temperatures during the same period, which benefits vegetation growth. The study area is relatively flat with an average altitude of approximately 24 m above sea level, thus reducing the uncertainties of LULC classification accuracy caused by topographical factors to a minimum. The area of this study region is approximately 45 km × 25 km (covered by two scenes of GF-2 multispectral data). Although it is not a very large region, it has the representative characteristics of LULC distribution in the North China Plain. The main LULC type is cropland, which is dominated by winter wheat. Winter wheat season begins in early October, and winter wheat is harvested in early June of the following year. In addition, a small quantity of vegetables is also planted in the croplands. There are also other LULC types, such as water bodies, bare lands, woodlands, and artificial construction.

To determine the actual LULC distribution and determine a suitable classification system in the study area, a field survey was carried out from 10th May to 15th May 2016, with the reference to the GF-2 multispectral data. During the field survey, the details of the representative LULC types were recorded based on the high spatial resolution remote sensing data. Photographs of represen-

Table 1 The main technical specifications of GF-2 multispectral cameras

Payloads	Bands No.	Spectral range/μm	Spatial resolution/m	Swath width/km	Repetition cycle/day	Local time of descending node
Multispectral	1	0.45–0.52	4	45 (two cameras combined)	5 (when sideway)	10:30 AM
	2	0.52–0.59				
	3	0.63–0.69				
	4	0.77–0.89				

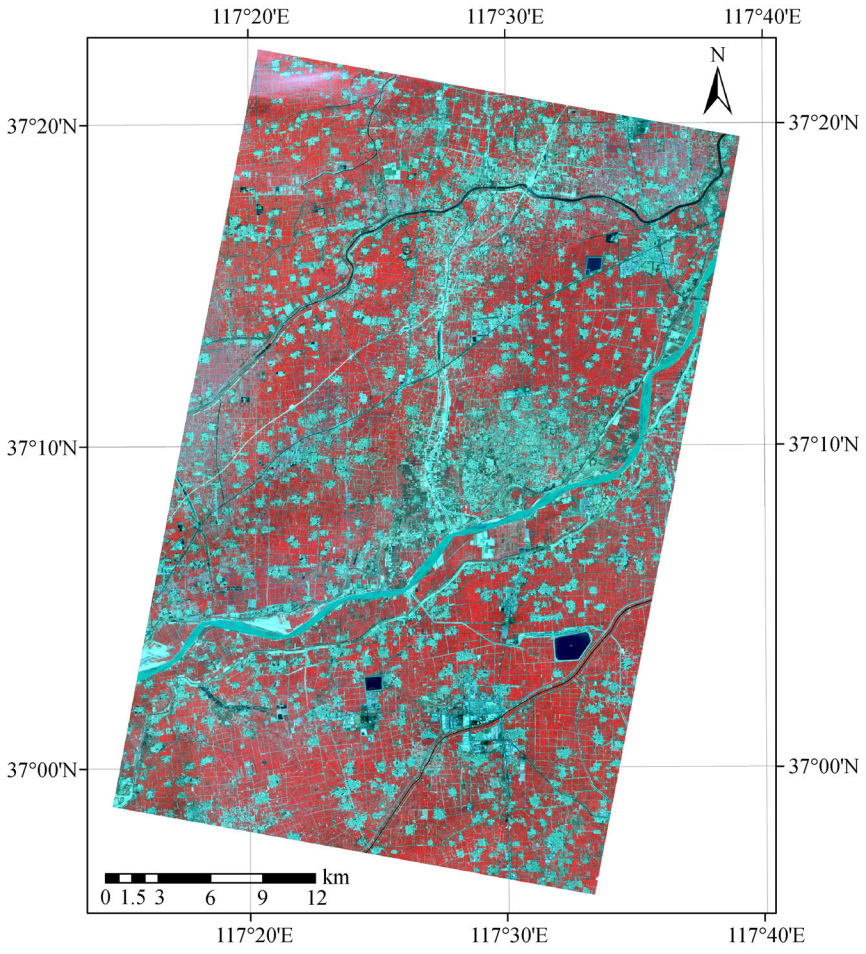

Fig. 1 The geographical location of the study area in the North China Plain. The image is the standard false color composited image (R: NIR, G: red, B: green) of GF-2 multispectral data acquired on April 5, 2016.

tative LULC types were collected using a digital camera, and the geographical positions were also recorded using a handheld global positioning system (GPS) receiver (Trimble Juno SB) with a positioning accuracy of ±3 m. The ground survey helped to determine the spatial LULC distribution characteristics in the study area and to identify the features of the different LULC types on the GF-2 multispectral image, which in turn helped to select the training and validating samples and to assist with the visual interpretation of the data.

Based on the field survey and considering agricultural type distribution being more important for agriculture monitoring in the North China Plain, five classes were identified: winter wheat, woodland, water, artificial surfaces, and vegetables. The artificial surface class type mainly included residential areas, construction lands, roads, and bare lands. Acquiring a representative sample collection is the most time-consuming and essential process in remote sensing data classification. In this study, samples were randomly selected from the known areas using the 'region of interest' (ROI) tools provided by ENVI version 5.0 software with the help of the aforementioned field survey and the GoogleEarth tool. To compare the classification results from the pixel-based and object-based classification strategies, it is better to use the same training and validation samples; thus, the samples were selected based on the segmentation results. These homogeneous sample regions were easily identified on the GF-2 multispectral image and the GoogleEarth map. The distribution of the sample regions was uniform, representing the entire study area. Half of the samples were randomly selected as the training samples, and the remaining half were used for classification accuracy validation. Finally, the total training sample pixels used for LULC classification were 2741 pixels for winter wheat, 4780 pixels for woodland, 27,162 pixels for water, 11,816 pixels for artificial surfaces, and 3472 pixels for vegetables. Because the samples were selected based on the segmentation results, there may be more sample pixels for a less distributed class in the study area. For example, the segmented objects of water bodies were usually very large because they exhibited concentrated distributions; thus, there were more sample pixels for water than for the other land use types.

3 Data and processing

Two adjacent scenes of cloud free GF-2 multispectral data covering the study area on 5th April 2016 were acquired from the China Centre for Resources Satellite Data and Application (CRESDA). The atmospheric conditions were good for the two data acquisition times and little smog appeared in the atmosphere; thus, the quality of the multispectral data was good (Fig. 1). The data were released in the form of a multiband digital number (DN) grid. The preprocessing of the GF-2 multispectral data contained radiance calibration, atmospheric correction, and geometric correction. The radiance calibration converted the DN values of the raw data to radiances using the following equation:

$$L_e = \text{Gain} \times \text{DN} + \text{Offset}, \quad (1)$$

where L_e is the radiance, and Gain and Offset are calibration coefficients obtained from the China Centre for Resources Satellite Data and Application.

The Fast Line-of-sight Atmospheric Analysis of Spectral Hypercubes (FLAASH) model was used to complete the atmospheric correction of the GF-2 multispectral data (Cooley et al., 2002). The input parameters for the FLAASH model were determined based on the imaging time and parameters of the two data. After atmospheric correction, the GF-2 land surface reflectance data were obtained and were used for LULC classification. The geometric correction of the data was conducted using a two-order polynomial transformation method with bilinear interpolation resampling. Because the ground control points were unavailable in this study area, high-quality Landsat-8 Operational Land Imager (OLI) data (Jia et al., 2014b) were downloaded from the United States Geological Survey (USGS) website as the base map to do the geometric correction. The ground control points were manually selected from the two images on obvious feature points, such as the road intersection points. Finally, an image mosaic of the atmospherically and geometrically corrected GF-2 multispectral data was conducted and the mosaic data were used to further investigate the performance of LULC classification using GF-2 multispectral data (Fig. 1).

4 Methods

4.1 LULC classification method

Two classification strategies, pixel-based and object-based, were used in LULC classification of the GF-2 multispectral data. The object-based classification, which segregated pixels into classes instead of single pixels, imitated the elements of human interpretation of remote sensing data. In the object-based classification, the most important procedure was to perform a good segmentation of the remote sensing data such that the objects were delineated clearly to characterize the landscape for the specific objective of interest (Zhang et al., 2014; Ma et al., 2017). The multiresolution segmentation method was performed in this study to delineate objects that represented different classes from the remote sensing data (Baatz and Schäpe, 2000; Benz et al., 2004; Zhang et al., 2014). It is usually difficult to find a certain agreement for setting an optimum scale for the segmentation (Ma et al., 2017); thus, multiple segmentation scales were tested to determine the optimum one in this study. The scales ranged from 10 to 100 with a step of 5, and the segmentation results were visually evaluated by experts to select the optimal scale. A segmentation scale of 25 was determined as the optimum segmentation parameter in this study.

To compare the performance of different classifiers, the commonly used maximum likelihood (MLC) and support vector machine (SVM) classifiers were selected for the pixel-based and object-based LULC classifications using GF-2 multispectral data. The MLC classifier was the most popular parametric classifier for remote sensing data classification (Foody et al., 1992; Jia et al., 2011), which assumed that a hyper-ellipsoid decision volume could be used to approximate the shape of the data clusters. For a given unknown pixel, the probability of membership in each class was calculated using the mean feature vectors of the classes, the covariance matrix, and the prior probability (Duda and Hart, 1973). The unknown pixel was classified as the class with the maximum probability of the membership. The SVM classifier was the widely used nonparametric machine learning classifier with no assumptions made regarding the underlying data distribution, which typically performed better in remote sensing data classification studies (Foody and Mathur, 2004; Pal and Mather, 2005; Jia et al., 2012; Pal and Foody, 2012). The SVM classifier obtains the optimal separating hyperplane for a training dataset in terms of the generalization error, and a detailed description of SVM can be found in Burges (1998). The radial basis function (RBF), which was usually used for the SVM classifier, was selected as the kernel function in this study (Jia et al., 2013). First, the RBF kernel function nonlinearly mapped samples into a higher dimensional space, thus the RBF could handle cases when the relationships between class types were not linear. Second, the RBF kernel function had fewer numerical computational difficulties. The penalty value C and kernel parameter γ were the two parameters used for the RBF kernel function, which were set to 100 and 0.25, respectively, according to prior experience. Therefore, there were four LULC classification methods investigated in this study, which included pixel-based classification using the MLC classifier, pixel-based classification using the SVM classifier, object-based classification using the MLC classifier, and object-based classification using the SVM classifier. In addition, the samples and the classifica-

tion features (only spectral features were used in this study) used for different classification methods were the same to ensure the LULC classification comparisons over uniform standards.

4.2 LULC classification accuracy assessment

To assess the LULC classification performance, the pixel-based and object-based classification results using the MLC and SVM classifiers were evaluated using visual observations and quantitative classification accuracy indicators. Randomly selected sample pixels, as described above, were used to quantitatively assess the LULC classification accuracy. The total numbers of sample pixels used for the classification accuracy assessment were 2741 pixels for winter wheat, 4780 pixels for woodland, 27,162 pixels for water, 11,816 pixels for artificial surfaces, and 3472 pixels for vegetables. The overall classification accuracy, producer's accuracy, user's accuracy, and kappa statistics were then estimated for quantitative classification performance analysis (Congalton and Green, 1999; Tso and Mather, 2001; Foody, 2009, 2013).

5 Results and discussion

5.1 LULC classification using GF-2 multispectral data

Pixel-based and object-based LULC classification results of the GF-2 multispectral data using the MLC and SVM classifiers are shown in Fig. 2, and a typical enlarged region is provided to show the detailed differences of different LULC classification results in Fig. 3. Based on the visual observations and expert's knowledge, each class type could be effectively identified and conformed to the actual LULC situations on the pixel-based and object-based classification results using both the MLC and SVM classifiers, which indicates satisfactory LULC classification results using the GF-2 multispectral data. Winter wheat is the main class type and is distributed throughout the study area (Fig. 2). Water bodies are correctly identified, and woodland is mainly distributed throughout the surrounding rivers and roads. The main difference between the pixel-based and object-based classification results is that land parcels in the object-based classification results are smoother and clearer, whereas some clear "salt and pepper" noises are presented in the pixel-based classification results (Fig. 3). For example, some pixels in one complete cropland parcel may be misclassified as other class types in the pixel-based classification results. Therefore, preliminary visual observations indicate that an object-based crop classification strategy is more suitable for GF-2 multispectral data. For different classifiers, they present some misclassifications between woodland and vegetables using MLC classifier, whereas those using SVM classifier are fewer. The SVM classifier performed with better results on classifying class types, which occupied small proportions in the study area, than the MLC classifier. Moreover, other studies have also demonstrated that the SVM classifier usually performs better for remote sensing data classification (Mountrakis et al., 2011).

5.2 LULC classification accuracy

The classification accuracy and kappa statistics were estimated based on the validation samples and the confusion matrixes of the GF-2 multispectral data pixel-based and object-based classification results using the SVM and MLC classifiers are shown in Tables 2–5, respectively. There were satisfactory LULC classification results for the GF-2 multispectral data based on both pixel-based and object-based classifications using both the MLC and SVM classifiers. The overall classification accuracies were all greater than 85%. For the MLC classifier, the overall performance of object-based classification result (overall accuracy 91.57%; kappa coefficient: 0.870) was superior to that of the pixel-based classification result (overall accuracy: 86.67%; kappa coefficient: 0.796). For the SVM classifier, the overall performance of object-based classification result (overall accuracy 94.33%; kappa coefficient: 0.911) was also superior to that of the pixel-based classification result (overall accuracy: 89.30%; kappa coefficient: 0.836). The classification accuracy assessments were the same as those for the visual observations, and the object-based classification using the same classifier could improve classification accuracy by approximately 5%, which further indicated that the object-based LULC classification strategy was more suitable for the GF-2 multispectral data. For the different classifiers, the SVM classifier achieved better classification accuracies than the MLC classifier using the same classification strategy, and the classification accuracy improvement by the SVM classifier was approximately 3% for both pixel-based and object-based classification results. Therefore, the object-based classification of GF-2 multispectral data using the SVM classifier achieved the best classification performance.

The user's and producer's accuracies of winter wheat in all the classification results are satisfactory, and the object-based classification using the SVM classifier also achieved the best performance with a user's accuracy of 85.48% and producer's accuracy of 93.43%. The most confused class type with winter wheat is vegetables, which is because the green vegetation during the growth period may present similar spectral characteristics in the GF-2 multispectral data. A better strategy to distinguish winter wheat from vegetables is to acquire multitemporal remote sensing data during the classification because winter wheat and vegetables usually have different phenological characteristics, and multitemporal remote sensing data can effectively distinguish these differences. Woodland also

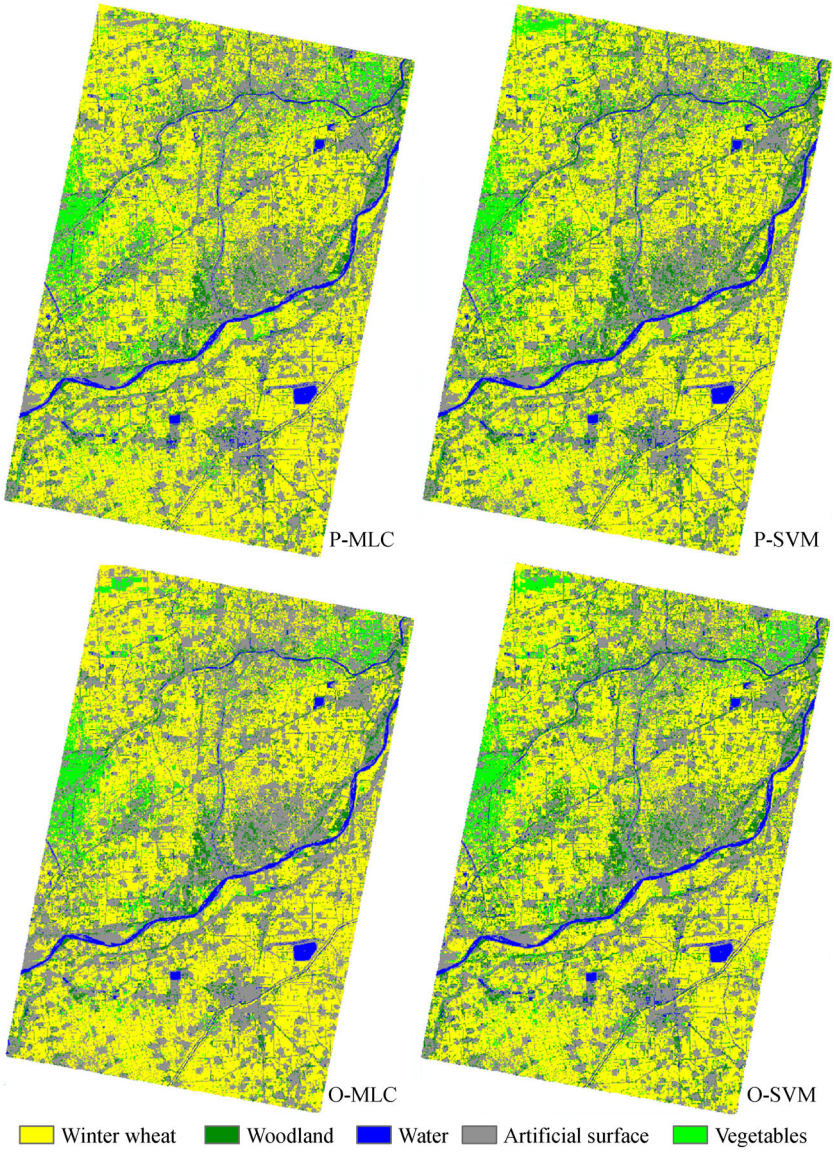

Fig. 2 Pixel-based and object-based LULC classification results of the GF-2 multispectral data using MLC and SVM classifiers, respectively (P-MLC: pixel-based classification using the MLC classifier, P-SVM: pixel-based classification using the SVM classifier, O-MLC: object-based classification using the MLC classifier, O-SVM: object-based classification using the SVM classifier).

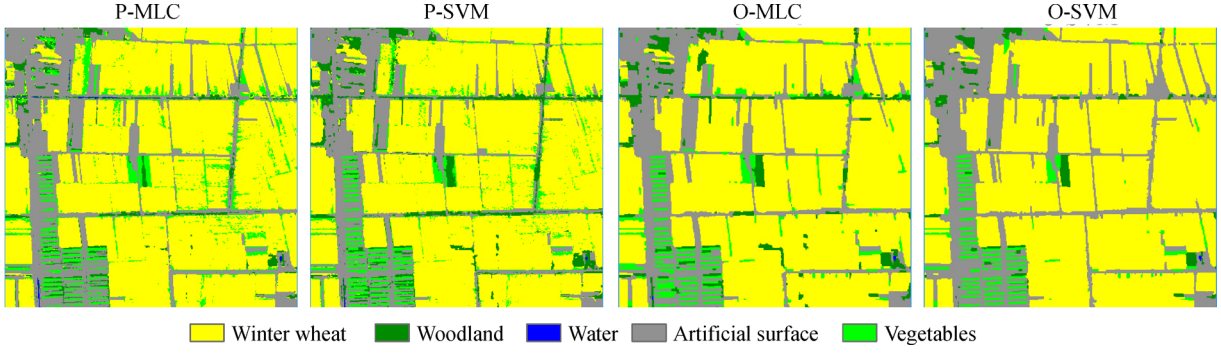

Fig. 3 A typical enlarged region (centered at 37°08′46″N, 117°24′6″E) to show the differences in the LULC classification results from different classification strategies (P-MLC: pixel-based classification using the MLC classifier, P-SVM: pixel-based classification using the SVM classifier, O-MLC: object-based classification using the MLC classifier, O-SVM: object-based classification using the SVM classifier).

Table 2 Confusion matrix for LULC classification of the GF-2 multispectral data using the pixel-based classification strategy and the MLC classifier. (OA: 86.67%, kappa coefficient: 0.796)

Mapped class	Ground truth/pixels						User accuracy
	Winter wheat	Woodland	Water	Artificial surface	Vegetables	Total	
Winter wheat	2372	46	0	1	439	2858	83.00%
Woodland	48	4003	29	171	60	4311	92.86%
Water	0	0	23,681	557	0	24,238	97.70%
Artificial surface	1	17	3452	10320	41	13,831	74.61%
Vegetables	320	714	0	767	2932	4733	61.95%
Total	2741	4780	27,162	11,816	3472	49,971	
Producer accuracy	86.54%	83.74%	87.18%	87.34%	84.45%		

Table 3 Confusion matrix for LULC classification of the GF-2 multispectral data using the pixel-based classification strategy and the SVM classifier (OA: 89.30%, kappa coefficient: 0.836)

Mapped class	Ground truth/pixels						User accuracy
	Winter wheat	Woodland	Water	Artificial surface	Vegetables	Total	
Winter wheat	2444	57	0	26	445	2972	82.23%
Woodland	32	4646	494	300	35	5507	84.37%
Water	0	0	23,989	303	0	24,292	98.75%
Artificial surface	0	5	2679	10,606	51	13,341	79.50%
Vegetables	265	72	0	581	2941	3859	76.21%
Total	2741	4780	27,162	11,816	3472	49,971	
Producer accuracy	89.16%	97.20%	88.32%	89.76%	84.71%		

Table 4 Confusion matrix for LULC classification of the GF-2 multispectral data using the object-based classification strategy and the MLC classifier (OA: 91.57%, kappa coefficient: 0.870)

Mapped class	Ground truth/pixels						User accuracy
	Winter wheat	Woodland	Water	Artificial surface	Vegetables	Total	
Winter wheat	2357	0	0	0	488	2845	82.85%
Woodland	0	4352	157	26	0	4535	95.96%
Water	0	34	24,922	137	0	25,093	99.32%
Artificial surface	57	0	2083	11,163	20	13,323	83.79%
Vegetables	327	394	0	490	2964	4175	70.99%
Total	2741	4780	27,162	11,816	3472	49,971	
Producer accuracy	85.99%	91.05%	91.75%	94.47%	85.37%		

presents some misclassification with winter wheat because some woodlands are shelterbelts located in the cropland boundaries and form the mixture pixels in the GF-2 multispectral data. Therefore, the minor misclassification between winter wheat and woodland is understandable.

In general, the classification results could indicate that the GF-2 multispectral data had a satisfactory performance on LULC classification in the study area, and the best strategy for LULC classification using GF-2 multispectral data was an object-based classification using the SVM classifier in this study. The GF-2 multispectral data also have many other potential application fields that should be explored in future work, such as vegetation parameter estimation, forest resource inventory, and water body extraction.

6 Conclusions

GF-2 is a new generation satellite of the China high-

Table 5 Confusion matrix for LULC classification of the GF-2 multispectral data using the object-based classification strategy and the SVM classifier (OA: 94.33%, kappa coefficient: 0.911)

Mapped class	Ground truth/pixels						User accuracy
	Winter wheat	Woodland	Water	Artificial surface	Vegetables	Total	
Winter wheat	2561	0	0	0	435	2996	85.48%
Woodland	6	4748	222	34	0	5010	94.77%
Water	0	0	25,689	330	0	6706	98.73%
Artificial surface	0	0	1251	11,122	20	12,393	89.74%
Vegetables	174	32	0	330	3017	3553	84.91%
Total	2741	4780	27,162	11,816	3472	49,971	
Producer accuracy	93.43%	99.33%	94.58%	94.13%	86.90%		

resolution earth observation system, which was successfully launched in August 2016 and began to supply high-resolution data for earth observations. This study explored the capability and strategy of GF-2 multispectral data for LULC classification in a region of the North China Plain. Pixel-based and object-based classifications using MLC and SVM classifiers were separately carried out to assess the LULC classification performance using GF-2 multispectral data. The validation results indicated satisfactory classification accuracy of GF-2 multispectral data, and the following primary conclusions could be drawn: 1) GF-2 multispectral data had a satisfactory performance in LULC classification in the study area of the North China Plain; 2) the object-based LULC classification strategy using the SVM classifier was more suitable for GF-2 multispectral data in this study. Therefore, considering the classification performance and sensor parameters, GF-2 satellite data could serve as a valuable high-resolution data source for land surface monitoring. Further work should focus on exploring the potential applications of GF-2 data on land surface monitoring, such as vegetation parameter estimation, and investigating the classification accuracy improvement by using multitemporal GF-2 data and more classification features.

Acknowledgements The authors would like to thank the anonymous reviewers and the editor for the constructive comments and suggestions, all of which have led to great improvements in the presentation of this article. This study was financially supported by the National Natural Science Foundation of China (Grant No. 41571422) and the National Key Research and Development Program of China (No. 2016YFA0600103). Kun Jia and Qiangzi Li conceived and designed the experiments; Kun Jia and Jingcan Liu performed the experiments and drafted the manuscript; Xiangqin Wei, Yunjun Yao, and Xiaotong Zhang supplied valuable suggestions on improving the method; Jingcan Liu, Yixuan Tu and Zhiwei Sun were responsible for field survey and classification accuracy assessment; All authors read and revised the manuscript. The authors declare no conflict of interest.

References

Adam E, Mutanga O, Odindi J, Abdel-Rahman E M (2014). Land-use/cover classification in a heterogeneous coastal landscape using RapidEye imagery: evaluating the performance of random forest and support vector machines classifiers. Int J Remote Sens, 35(10): 3440–3458

Aguilar M, Bianconi F, Aguilar F, Fernández I (2014). Object-based greenhouse classification from GeoEye-1 and WorldView-2 stereo imagery. Remote Sens, 6(5): 3554–3582

Baatz M, Schäpe M (2000). Multiresolution segmentation: an optimization approach for high quality multi-scale image segmentation. In: Strobl J, Blaschke T, Griesebner G, eds. Angewandte Geographische Informations-Verarbeitung XII. Karlsruhe: Wichmann Verlag, 12–23

Benz U C, Hofmann P, Willhauck G, Lingenfelder I, Heynen M (2004). Multi-resolution, object-oriented fuzzy analysis of remote sensing data for GIS-ready information. ISPRS J Photogramm Remote Sens, 58(3–4): 239–258

Burges C J C (1998). A tutorial on support vector machines for pattern recognition. Data Min Knowl Discov, 2(2): 121–167

Chen J, Chen J, Liao A, Cao X, Chen L, Chen X, He C, Han G, Peng S, Lu M, Zhang W, Tong X, Mills J (2015). Global land cover mapping at 30 m resolution: a POK-based operational approach. ISPRS J Photogramm Remote Sens, 103: 7–27

Congalton R G, Green K (1999). Assessing the Accuracy of Remotely Sensed Data: Principles and Practices. Florida: Lewis Publishers

Cooley T, Anderson G P, Felde G W, Hoke M L, Ratkowski A J, Chetwynd J H, Gardner J A, Adler-Golden S M, Matthew M W, Berk A, Bernstein L S, Acharya P K, Miller D, Lewis P (2002). FLAASH, a MODTRAN4-based atmospheric correction algorithm, its application and validation. In: 2002 IEEE International Geoscience and Remote Sensing Symposium & 24th Canadian Symposium on Remote Sensing. Toronto, Canada: IEEE Press

Duda R O, Hart P E (1973). Pattern Classification and Scene Analysis. New York: Wiley

Foody G M (2009). Classification accuracy comparison: hypothesis tests and the use of confidence intervals in evaluations of difference, equivalence and non-inferiority. Remote Sens Environ, 113(8): 1658–1663

Foody G M (2013). Ground reference data error and the mis-estimation of the area of land cover change as a function of its abundance. Remote Sens Lett, 4(8): 783–792

Foody G M, Campbell N A, Trodd N M, Wood T F (1992). Derivation and applications of probabilistic measures of class membership from

the maximum-likelihood classification. Photogramm Eng Remote Sensing, 58: 1335–1341

Foody G M, Mathur A (2004). A relative evaluation of multiclass image classification by support vector machines. IEEE Trans Geosci Remote Sens, 42(6): 1335–1343

Friedl M A, Brodley C E (1997). Decision tree classification of land cover from remotely sensed data. Remote Sens Environ, 61(3): 399–409

Gebbers R, Adamchuk V I (2010). Precision agriculture and food security. Science, 327(5967): 828–831

Gong P, Wang J, Yu L, Zhao Y C, Zhao Y Y, Liang L, Niu Z G, Huang X M, Fu H H, Liu S, Li C C, Li X Y, Fu W, Liu C X, Xu Y, Wang X Y, Cheng Q, Hu L Y, Yao W B, Zhang H, Zhu P, Zhao Z Y, Zhang H Y, Zheng Y M, Ji L Y, Zhang Y W, Chen H, Yan A, Guo J H, Wang L, Liu X J, Shi T T, Zhu M H, Chen Y L, Yang G W, Tang P, Xu B, Giri C, Clinton N, Zhu Z L, Chen J, Chen J (2013). Finer resolution observation and monitoring of global land cover: first mapping results with Landsat TM and ETM + data. Int J Remote Sens, 34(7): 2607–2654

Gong P, Yu L, Li C, Wang J, Liang L, Li X, Ji L, Bai Y, Cheng Y, Zhu Z (2016). A new research paradigm for global land cover mapping. Ann GIS, 22(2): 87–102

Hansen M C, Defries R S, Townshend J R G, Sohlberg R (2000). Global land cover classification at 1 km spatial resolution using a classification tree approach. Int J Remote Sens, 21(6–7): 1331–1364

Jia K, Li Q Z, Tian Y C, Wu B F, Zhang F F, Meng J H (2012). Crop classification using multi-configuration SAR data in the North China Plain. Int J Remote Sens, 33(1): 170–183

Jia K, Liang S, Zhang N, Wei X Q, Gu X F, Zhao X, Yao Y J, Xie X (2014a). Land cover classification of finer resolution remote sensing data integrating temporal features from time series coarser resolution data. ISPRS J Photogramm Remote Sens, 93: 49–55

Jia K, Wei X Q, Gu X F, Yao Y J, Xie X H, Li B (2014b). Land cover classification using Landsat 8 Operational Land Imager data in Beijing, China. Geocarto Int, 29(8): 941–951

Jia K, Wu B F, Li Q Z (2013). Crop classification using HJ satellite multispectral data in the North China Plain. J Appl Remote Sens, 7 (1): 073576

Jia K, Wu B F, Tian Y C, Zeng Y, Li Q Z (2011). Vegetation classification method with biochemical composition estimated from remote sensing data. Int J Remote Sens, 32(24): 9307–9325

Li Q, Cao X, Jia K, Zhang M, Dong Q (2014). Crop type identification by integration of high-spatial resolution multispectral data with features extracted from coarse-resolution time-series vegetation index data. Int J Remote Sens, 35(16): 6076–6088

Liang S (2008). Advances in Land Remote Sensing System, Modeling Inversion and Application. Dordrecht: Springer

Liu J Y, Liu M L, Zhuang D F, Zhang Z X, Deng X Z (2003). Study on spatial pattern of land-use change in China during 1995–2000. Sci China Ser D Earth Sci, 46: 373–384

Lu D, Weng Q (2007). A survey of image classification methods and techniques for improving classification performance. Int J Remote Sens, 28(5): 823–870

Ma L, Li M, Ma X, Cheng L, Du P, Liu Y (2017). A review of supervised object-based land-cover image classification. ISPRS J Photogramm Remote Sens, 130: 277–293

Mathur A, Foody G (2008). Crop classification by support vector machine with intelligently selected training data for an operational application. Int J Remote Sens, 29(8): 2227–2240

Miller S N, Phillip Guertin D, Goodrich D C (2007). Hydrologic modeling uncertainty resulting from land cover misclassification. J Am Water Resour Assoc, 43(4): 1065–1075

Mountrakis G, Im J, Ogole C (2011). Support vector machines in remote sensing: a review. ISPRS J Photogramm Remote Sens, 66(3): 247–259

Pal M, Foody G M (2012). Evaluation of SVM, RVM and SMLR for accurate image classification with limited ground data. IEEE J Sel Top Appl Earth Obs Remote Sens, 5(5): 1344–1355

Pal M, Mather P M (2005). Support vector machines for classification in remote sensing. Int J Remote Sens, 26(5): 1007–1011

Running S W (2008). Ecosystem disturbance, carbon, and climate. Science, 321(5889): 652–653

Schmidt M, Pringle M, Devadas R, Denham R, Tindall D (2016). A framework for large-area mapping of past and present cropping activity using seasonal Landsat images and time series metrics. Remote Sens, 8(4): 312

Tso B, Mather P M (2001). Classification Methods for Remotely Sensed Data. London: Taylor and Francis

Yan L, Roy D P (2016). Conterminous United States crop field size quantification from multi-temporal Landsat data. Remote Sens Environ, 172: 67–86

Yang J, Gong P, Fu R, Zhang M H, Chen J M, Liang S L, Xu B, Shi J C, Dickinson R (2013). The role of satellite remote sensing in climate change studies. Nat Clim Chang, 3(10): 875–883

Yu L, Su J, Li C, Wang L, Luo Z, Yan B (2018). Improvement of moderate resolution land use and land cover classification by introducing adjacent region features. Remote Sens, 10(3): 414

Zhang H, Li Q, Liu J, Shang J, Du X, Zhao L, Wang N, Dong T (2017). Crop classification and acreage estimation in North Korea using phenology features. GISci Remote Sens, 54(3): 381–406

Zhang L, Jia K, Li X S, Yuan Q Z, Zhao X F (2014). Multi-scale segmentation approach for object-based land-cover classification using high-resolution imagery. Remote Sens Lett, 5(1): 73–82

Zhang M W, Zhou Q B, Chen Z X, Liu J, Zhou Y, Cai C F (2008). Crop discrimination in northern China with double cropping systems using Fourier analysis of time-series MODIS data. Int J Appl Earth Obs Geoinf, 10(4): 476–485

Zhong L, Hu L, Yu L, Gong P, Biging G S (2016). Automated mapping of soybean and corn using phenology. ISPRS J Photogramm Remote Sens, 119: 151–164